Biophysical Journal, Volume *111*

Supplemental Information

Background Suppression in Imaging Gold Nanorods through Detection of Anti-Stokes Emission

Aquiles Carattino, Veer I.P. Keizer, Marcel J.M. Schaaf, and Michel Orrit

Background suppression in imaging gold nanorods through detection of anti-Stokes emission

A. Carattino, V.I.P. Keizer, M.J.M Schaaf, and M. Orrit

E-mail:

Setup

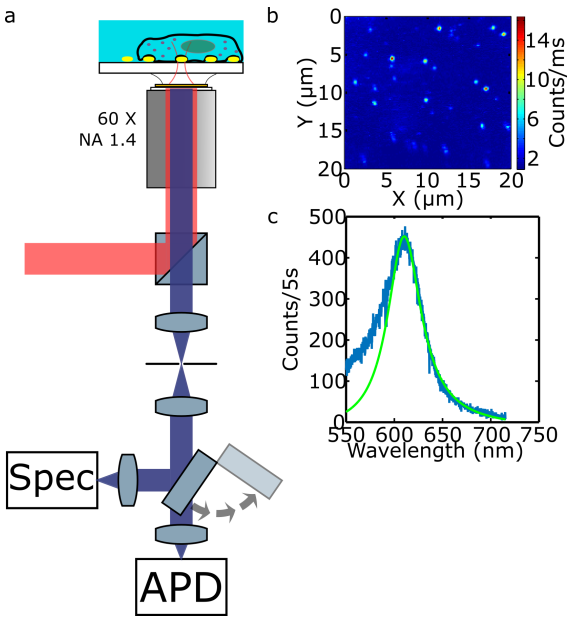

Figure S1: Experimental setup and examples of observations. a) Simplified schematic of the confocal microscope employed during the measurements. b) A typical 1-photon luminescence raster scan of the sample immersed in water c) luminescence spectrum of a single rod.

Figure S1 shows the schematic of the confocal microscope employed in the experiments. It is important to note the presence of a 50/50 beamsplitter before the objective. Exchanging

it for an appropriate dichroic mirror would increase the collection efficiency. In this work we chose not to do it because the beamsplitter allows to collect both the full emission under 532 nm excitation and the Stokes/anti-Stokes emission under 633 nm without changes in the optical path.

Uv-Vis spectrum

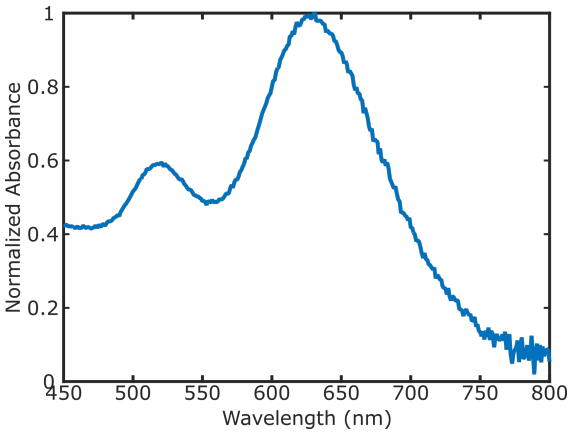

Figure S2: Normalized extinction spectrum of a suspension of nanorods after synthesis. The resonance maximum is located at 630 nm.

Figure S2 shows the extinction spectrum of the nanorod samples used throughout this work. Two peaks are clearly distinguishable, one around 630 nm that corresponds to the longitudinal plasmon resonance (LPR) of particles with sizes 50 nm × 23 nm and a second one at around 520 nm. This peak also includes contributions of spheres as by-products of the synthesis of the rods. The transverse plasmon resonance is also located at the same wavelength but is much weaker than the LPR. In a sample consisting exclusively of rods, the transverse resonance would be barely observable in a UV-Vis spectrometer.

Filters

The selection of filters plays a crucial role in the signal acquired. Since the main part of the anti-Stokes emission is concentrated around the excitation wavelength, it is important

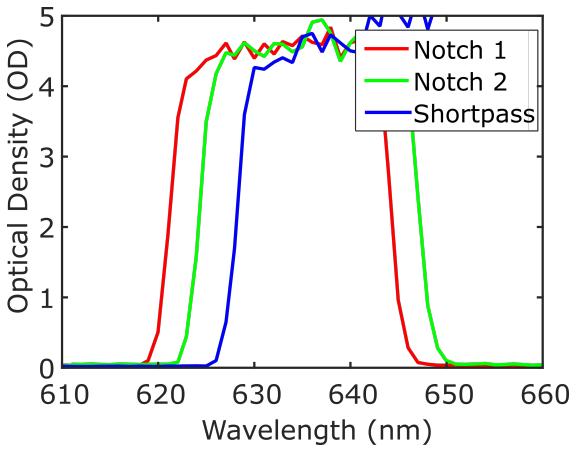

Figure S3: Transmission spectrum of two notch filters and a short pass filter (Semrock).

to select filters that have a high transmission close to the laser line. Figure S3 shows the normalized absorption spectrum of two notch filters and a short pass. Both notch filters are branded as NF03 − 633E − 25 but show a slightly different absorption spectrum, shifted roughly 4 nm from each other. The shortpass filter (branded as SP01 − 633RU − 25) shows the transition to transmission even closer to the laser line.

For many fluorescence applications the exact shape of the transmission spectrum of the filters does not play a crucial role. However for anti-Stokes imaging, since the shape of the emission is exponential-like, minute changes in the transmission spectrum can have a great impact on the signal collected. For example, changing from a detection path with a spectrum like notch 1 to one like shortpass (i.e. shifting in about 7 nm the edge of the filter) increases the collected number of photons by about 50%.

In this work, since only one filter does not provide enough attenuation, care was taken to always employ the notch with the most favorable transmission spectrum in combination with either a shortpass or a longpass filter. Ideally, two shortpass filters would have been the best solution.

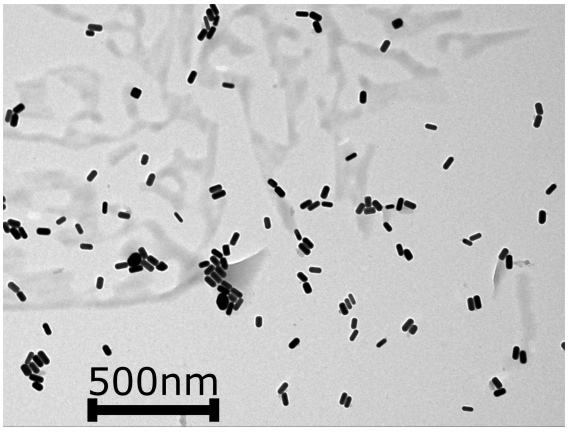

Figure S4: TEM image of the nanorod sample. The scale bar is 500 μm.

TEM Images of rods

Figure S4 shows an example TEM image of the gold nanorod sample. Analysis on the dimensions of the particles yield an average length of 50 nm and diameter of 23 nm. This is consistent with the plasmon observed in fig. S2 and at a single-particle level as in fig. S1c.

White light transmission

Full scan without dye

The raster scan shown in Figure S6 corresponds to a larger area comprising the same region shown in the main text. The majority of the particles has a much larger contrast in the anti-Stokes. Moreover it can be noted that the background is flat. In the Stokes image the nanorods are still visible, but the contrast is obviously lower.

Full scan without dye

Figure S7 shows a raster scan of gold nanorods under cells stained with Atto 647N. Both images comprise the same region shown in the main text, here marked with a black square. No particles can be detected in the Stokes image, while several nanorods are visible in the

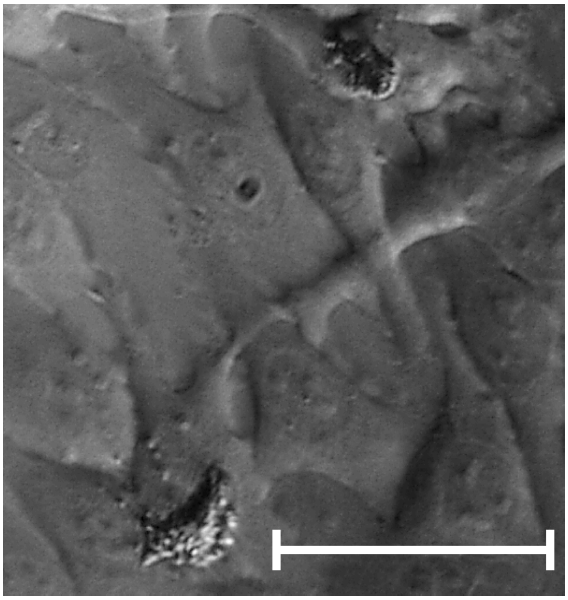

Figure S5: White light transmission image of the sample with cells deposited on top of the rods. It is possible to observe that they cover entirely the observed region without spacing in between them. The scale bar in the figure is 20 μm in length.

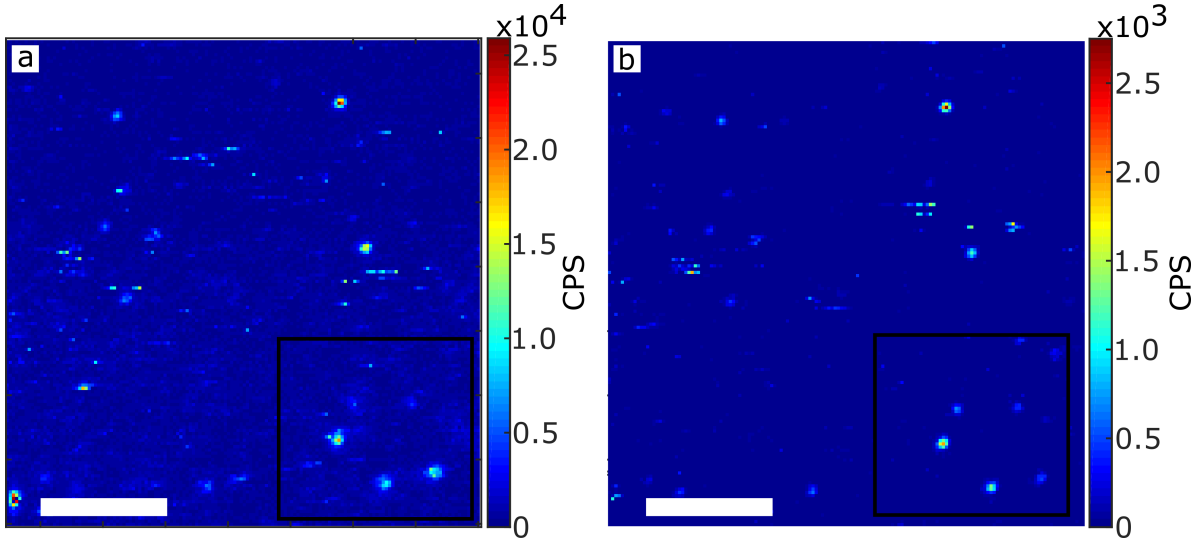

Figure S6: Raster scan of a nanorod sample under HeLa cells using (a) a long pass filter and (b) a short pass filter for photoluminescence detection. Both scans contain the same region shown in the main text and here marked with a black square. The scale bar in both figures is 4 μm in length.

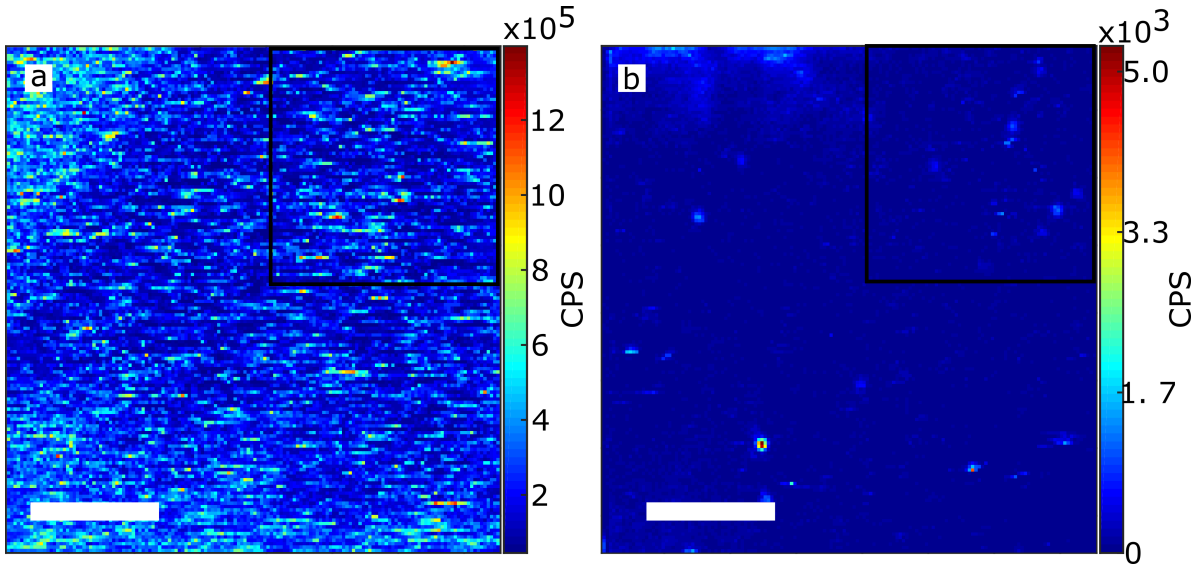

Figure S7: Raster scan of a nanorod sample under stained HeLa cells using (a) a long pass filter and (b) a short pass filter for photoluminescence detection. Both scans contain the same region shown in the main text and here marked with a black square. The scale bar in both figures is 4 μm in length.

anti-Stokes image with a high signal-to-background. We note, however, that there is some background appearing in the top left part of the anti-Stokes image. This may be due to an increase of the concentration of Atto 647N. The incubation procedure does not prevent the accumulation of dye in specific organelles of the cells, and there is no control on the final dye concentration.

Signal-to-background of several particles

Figure S8 shows the distribution of signal-to-background ratios for several particles. The data were acquired with an irradiation intensity of 30 kW/cm^2. Fig. S8a shows the distribution for nanoparticles under unstained cells. It is possible to observe a broad distribution of values between ratios of 5 and 15. Fig. S8b shows the signal-to-background distribution for the anti-Stokes emission, concentrated mainly between 5 and 10. Finally Figure S8c shows the anti-Stokes signal-to-background ratio of particles under cells stained with Atto 647N. In this case it is possible to observe a similar distribution of values. Stokes data under stained

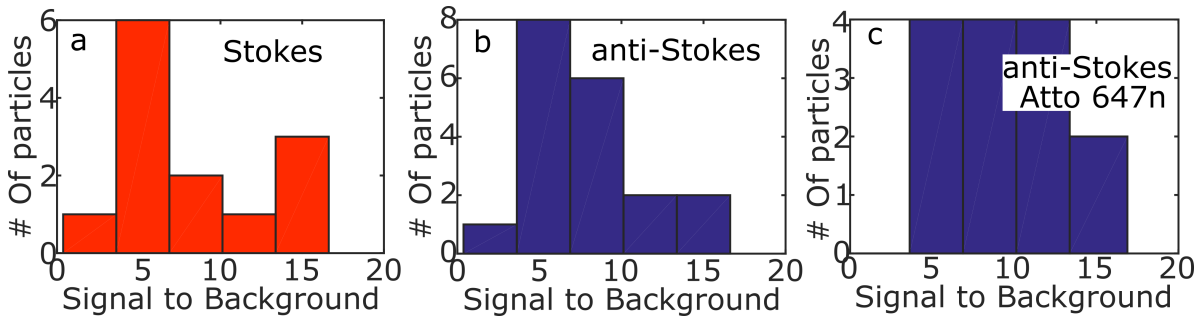

Figure S8: Histograms of the signal-to-background of several particles irradiated at $30\,\mathrm{kW/cm^2}$. a) Stokes emission under unstained cells, b) same but anti-Stokes emission, c) anti-Stokes under cells stained with Atto 647N.

cells are not presented because it was impossible to detect single nanoparticles under those conditions.

Viability test

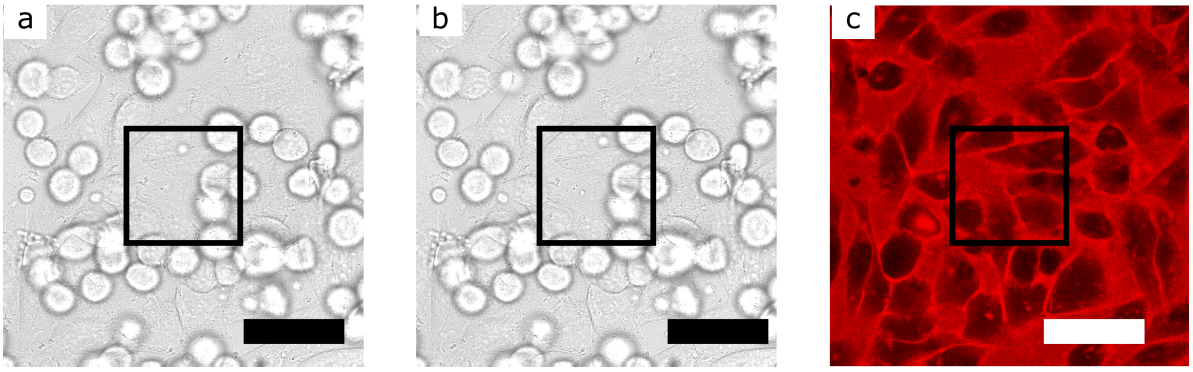

Figure S9: White light transmission image of the cells, a) before being irradiated with the 633 nm laser, b) after the imaging process and c) viability test. The black square represents the imaged area. The scale bar is $50\,\mu\mathrm{m}$.

To support the claim of the harmlessness of the method proposed in this work, we performed a standard viability test of the cells after imaging. Figure S9 shows white light transmission images of the cells. The left figure is before the imaging of the nanorods, the central is after and the rightmost is the result of a viability test with trypan blue. The black square represents the area that was imaged with the confocal microscope. The cells show no change between before and after the procedure. Moreover in Fig. S9c it is possible to see

that the dye did not enter the cells, therefore their membrane was intact after the imaging process.

More rigorous tests of viability after imaging the nanorods inside the cells are needed, but they are outside the scope of this work. On one hand there is enough evidence showing that gold nanoparticles are not toxic for cells.[1,2] On the other hand two photon imaging[3] or photothermal heterodyne detection[4] of particles inside cells did not destroy them. Continuous wave confocal imaging as presented here however was not studied in detail in the past mainly because of the poor signal-to-background ratio with the normal Stokes configuration.

References

(1) Huff, T. B.; Hansen, M. N.; Zhao, Y.; Cheng, J.-x.; Wei, A. Controlling the Cellular Uptake of Gold Nanorods. *Langmuir* **2007**, *23*, 1596–1599.

(2) Lewinski, N.; Colvin, V.; Drezek, R. Cytotoxicity of nanopartides. *Small* **2008**, *4*, 26–49.

(3) van den Broek, B.; Ashcroft, B.; Oosterkamp, T. H.; van Noort, J. Parallel Nanometric 3D Tracking of Intracellular Gold Nanorods Using Multifocal Two-Photon Microscopy. *Nano Lett.* **2013**, *13*, 980–986.

(4) Leduc, C.; Si, S.; Gautier, J.; Soto-Ribeiro, M.; Wehrle-Haller, B.; Gautreau, A.; Giannone, G.; Cognet, L.; Lounis, B. A highly specific gold nanoprobe for live-cell single-molecule imaging. *Nano Lett.* **2013**, *13*, 1489–94.